Enhancement of CO Insertion into a Pd−C Bond in a Pd−Co Heterodinuclear Complex

Atsushi Fukuoka,[†,‡] Sumiko Fukagawa,[†] Masafumi Hirano,[†] Nobuaki Koga,[§] and Sanshiro Komiya*[,†]

Department of Applied Chemistry, Tokyo University of Agriculture and Technology, 2-24-16 Nakacho, Koganei, Tokyo 184-8588, Japan, and Graduate School of Human Informatics, Nagoya University, Nagoya 464-8601, Japan

Received December 5, 2000

A series of Pd-containing heterodinuclear methyl complexes, (dppe)(CH_3)Pd−ML_n (ML_n = $MoCp(CO)_3$, $WCp(CO)_3$, $Co(CO)_4$; dppe = 1,2-bis(diphenylphosphino)ethane), have been prepared by the metathetical reactions of Pd$(CH_3)(NO_3)$(dppe) with $Na^+[ML_n]^-$, and the complexes were characterized by spectroscopic methods and/or X-ray structure analysis. Related Pt-containing dinuclear complexes were similarly prepared and characterized. The rate of CO insertion into a Pd−CH_3 or Pt−CH_3 bond was investigated using these complexes. The Pd−Co complex (dppe)(CH_3)Pd−$Co(CO)_4$ shows a high activity of CO insertion, giving (dppe)(CH_3CO)Pd−$Co(CO)_4$, and the initial rate is ca. 80 times higher than those of the analogous complex Pd(CH_3)Cl(dppe). Whereas slow insertion of CO is observed in the Pt−Co complex (dppe)(CH_3)Pt−$Co(CO)_4$, no reaction takes place for Pt(CH_3)Cl(dppe). It is revealed by using ^{13}CO that CO in the $Co(CO)_4$ fragment preferentially inserts into the Pd−CH_3 bond over CO in the gas phase. The carbonyl insertion reaction in the Pd−Co heterodinuclear complex has been theoretically studied using B3LYP hybrid density functional theory to clarify its reaction mechanism and the electronic factors controlling the reaction. The calculations for a model complex, $(H_2PCH_2CH_2PH_2)$Pd(CH_3)−$Co(CO)_4$, have shown that the most favorable reaction path consists of methyl migration from the Pd to the Co atom, carbonyl insertion reaction on the Co atom, CO coordination to the Co atom, and acetyl migration from the Co atom to the Pd atom, which is in accord with the experimental results. The electron donation from the Pd d orbital to the bridging CO π^* orbitals plays an important role in stabilizing the intermediates and transition states.

Introduction

In transition-metal-catalyzed C−C bond formation reactions,[1] Pd complexes play an important role in CO-related reactions such as single and double carbonylation of aryl halide[2] and copolymerization of CO with alkenes.[3] In these catalytic carbonylation reactions, CO insertion into the Pd−alkyl or Pd−aryl bonds is a key elemental reaction to form C−C bonds, and monometallic Pd complexes are widely used with fine-tuning of coordinated ligands. Moreover, it has recently been reported that Pd-containing bimetallic catalysts show unique catalytic activities in carbonylation reactions, which is not observed in the monometallic Pd catalysis. Hidai et al. described that Pd−Co catalysts exhibited high activity in the carbonylation of aryl iodide and that the Pd−Co heterodinuclear acyl complex *trans*-$((CH_3)_3P)_2$-$(C_6H_5C(O))$Pd−$Co(CO)_4$ was formed from the reaction of $Pd(C_6H_5)(OTf)(P(CH_3)_3)_2$ with $K^+[Co(CO)_4]^-$.[4] Braunstein et al. reported the copolymerization of CO with norbornene on a Pd−Fe dinuclear complex.[5]

Heterodinuclear complexes and heterobimetallic cluster complexes have attracted much attention, since they may show a synergistic effect of different metal centers on the reactivity of organic ligands such as alkyl and aryl groups.[6] Many papers have reported the synergistic effect of two different metals in catalytic and stoichiometric transformations on the dinuclear or cluster

* To whom correspondence should be addressed. E-mail: komiya@cc.tuat.ac.jp.
[†] Tokyo University of Agriculture and Technology.
[‡] Present address: Catalysis Research Center, Hokkaido University, Sapporo 060-0811, Japan.
[§] Nagoya University.

(1) (a) Collman, J. P.; Hegedus, L. S.; Norton, J. R.; Finke, R. G. *Principles and Applications of Organnotransition Metal Chemistry*; University Science Books: Mill Valley, CA, 1987. (b) Yamamoto, A. *Organotransition Metal Chemistry*; Wiley-Interscience: New York, 1986. (c) Crabtree, R. H. *The Organometallic Chemistry of the Transition Metals*; Wiley-Interscience: New York, 1994. (d) Parshall, G. W.; Ittel, S. D. *Homogeneous Catalysis*; 2nd ed.; Wiley-Interscience: New York, 1992. (e) Cornils, B., Herrmann, W. A., Eds. *Applied Organometallic Catalysis with Organometallic Compounds*; VCH: Weinheim, Germany, 1996.

(2) (a) Shoenberg, A.; Bartoletti, I.; Heck, R. F. *J. Org. Chem.* **1974**, *39*, 3318−3326. (b) Hidai, M.; Hikita, T.; Wada, Y.; Fujikura, Y.; Uchida, Y. *Bull. Chem. Soc. Jpn.* **1975**, *48*, 2075−2077. (c) Ozawa, F.; Soyama, H.; Yamamoto, T.; Yamamoto, A. *Tetrahedron Lett.* **1982**, *23*, 3383−3386. (d) Kobayashi, T.; Tanaka, M. *J. Organomet. Chem.* **1982**, *233*, C64−C66. (e) Yamamoto, A. *Bull. Chem. Soc. Jpn.* **1995**, *68*, 433−446.

(3) (a) Sen, A.; Lai, T.-W. Z. *J. Am. Chem. Soc.* **1982**, *104*, 3520−3522. (b) Sen, A. *Acc. Chem. Res.* **1993**, *26*, 303−310. (c) Drent, E. Eur. Pat. Appl. 121,965, 1984. (d) Drent, E.; van Broekhoven, J. A. M.; Budzulaar, P. H. M. In ref 3e, p 333. (e) Nozaki, K.; Sato, N.; Takaya, H. *J. Am. Chem. Soc.* **1995**, *117*, 9911−9912.

(4) Misumi, Y.; Ishii, Y.; Hidai, M. *J. Chem. Soc., Dalton Trans.* **1995**, 3489−3496.

(5) Braunstein, P.; Knorr, M.; Stährfekdt, T. *J. Chem. Soc., Chem. Commun.* **1994**, 1913−1914.

10.1021/om001037v CCC: $20.00
Publication on Web 04/19/2001

complexes. However, there are fewer examples that elucidate the origin of synergism at the molecular level.

In our study of the synthesis and reactivity of Pt-containing heterodinuclear complexes $L_2RPt-ML_n$ (L_2 = 1,5-cyclooctadiene (cod), dppe; R = alkyl, aryl; ML_n = $MoCp(CO)_3$, $WCp(CO)_3$, $Mn(CO)_5$, $FeCp(CO)_2$, $Co(CO)_4$), we have demonstrated that reductive elimination and β-H elimination are greatly enhanced on the Pt−M heterodinuclear complexes in comparison to the mononuclear Pt complex.[7] In the present work, we extended our research to the chemistry of Pd-containing heterodinuclear complexes, since the Pd−M complexes are expected to show higher catalytic activity than the corresponding Pt−M complexes. We have synthesized new Pd−M heterodinuclear complexes with a CH_3 group, and the CO insertion into the $Pd-CH_3$ bonds on the Pd−M complexes has been studied experimentally and theoretically. The CO insertion reaction on the Pd−Co complex is markedly enhanced owing to the heterodinuclear structure, and the reaction mechanism is elucidated by the theoretical calculations. A part of this work was given in a preliminary report.[7f]

Results and Discussion

Synthesis and Characterization of Heterodinuclear Complexes. Metathetical reactions of $Pd(CH_3)(NO_3)$(dppe), prepared in situ from $Pd(CH_3)Cl$(dppe) (**1**) and $AgNO_3$, with a slight excess of $Na^+[ML_n]^-$ in THF at −30 °C under N_2 gave the new dinuclear complexes $(dppe)(CH_3)Pd-ML_n$ (ML_n = $MoCp(CO)_3$ (**2**), $WCp(CO)_3$ (**3**), $Co(CO)_4$ (**4**)) (eq 1). When spectroscopic

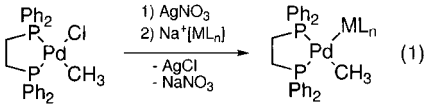

and analytical data of **2**−**4** are compared with those of the related Pt analogues $(dppe)(CH_3)Pt-ML_n$,[7c] it is established that **2**−**4** have similar dinuclear structures with a methyl group on Pd, as shown in eq 1. Elemental analyses gave satisfactory results for **2** and **4**. The molar electric conductivities of **2**−**4** were significantly low, showing that they are not ionic but neutral complexes.

Selected NMR and IR data of **2**−**4** are listed in the Experimental Section. Typically, the ^1H NMR spectrum of $(dppe)(CH_3)Pd-Co(CO)_4$ (**4**) gave a doublet of doublets at δ 1.21 due to the methyl group coupled to two phosphorus nuclei of dppe ($^3J_{PH}$ = 7.7, 5.0 Hz). In the $^{31}P\{^1H\}$ NMR spectrum of **4**, the dppe resonances were observed at δ 37.2 and 49.4 as two doublets ($^2J_{PP}$ = 26 Hz). These results show that the two P nuclei of dppe are not magnetically equivalent, implying a square-planar geometry around Pd. The IR spectrum of **4** gave four ν(CO) bands at 2020, 1953, 1913, and 1885 cm^{-1}, which are similar to those for −I valent $Na^+[Co(CO)_4]^-$ (2002 cm^{-1}). We infer that the oxidation states of the metals are close to Pd(II) and Co(−I), although the formal oxidation states are Pd(I) and Co(0) in the bimetallic structure with a direct Pd−Co bond. The presence of the Pd−Co bond has been confirmed by X-ray crystallography, as described below.

Table 1. Selected Bond Distances (Å) and Angles (deg) for 5

Pt−Co	2.676(2)	Pt−P(1)	2.313(5)
Pt−P(2)	2.235(4)	Pt−C(1)	2.12(2)
Pt−C(2)	2.66(2)	Pt−C(3)	4.24(2)
Pt−C(4)	2.64(2)	Pt−C(5)	3.73(2)
Co−C(2)	1.79(2)	Co−C(3)	1.79(2)
Co−C(4)	1.81(2)	Co−C(5)	1.81(2)
Co−Pt−P(1)	100.4(1)	Co−Pt−C(1)	85.7(4)
P(1)−Pt−P(2)	85.5(2)	P(2)−Pt-C(1)	88.3(5)
Co−C(2)−O(1)	174(1)	Co−C(3)−O(2)	177(2)
Co−C(4)−O(3)	170(1)	Co−C(5)−O(4)	177(2)

The molecular structures of the Pd−Co complex **4**[8] and its Pt−Co analogue $(dppe)(CH_3)Pt-Co(CO)_4$[7c] (**5**) were determined by single-crystal X-ray structure analyses. ORTEP drawings of **4** and **5** are depicted in Figure 1, and selected bond distances and angles for **5** are listed in Table 1. The Pd−Co distance for **4** is 2.682(8) Å, which is slightly shorter than that for $((CH_3)_3P)_2(C_6H_5C(O))Pd-Co(CO)_4$ (2.7856(7) Å).[4] This result unequivocally demonstrates the presence of a Pd−Co single bond in **4**. The molecular structure of the corresponding Pt−Co complex **5** is basically isomorphous with **4**, and the axial C(4)−O(3) and C(2)−O(1) carbonyls are slightly bent, indicating a weak semibridging interaction with Pt: Pt−C(4) = 2.64(2) Å and Co−C(4)−O(3) = 170(1)°; Pt−C(2) = 2.66(2) Å and Co−C(2)−O(1) = 174(1)°.

CO Insertion Reaction into the Pd−CH_3 Bond. The reactivity of the new heterodinuclear complexes toward CO insertion was investigated. Treatment of the Pd−Co complex **4** with atmospheric CO in benzene at room temperature led to the formation of an acetyl complex, $(dppe)(CH_3C(O))Pd-Co(CO)_4$ (**6**), in 16 h (eq 2).

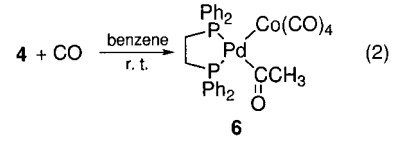

Complex **6** was isolated as orange needles in 85% yield by recrystallization from a mixture of benzene and hexane. Under the same reaction conditions, the Pd−

(6) (a) Braunstein, P., Oro, L. A., Raithby, P. R., Eds. *Metal Clusters in Chemistry*; Wiley-VCH: Weinheim, Germany, 1999. (b) Adams, R. D., Cotton, F. A., Eds. *Catalysis by Di- and Polynuclear Metal Cluster Complexes*; Wiley-VCH: New York, 1998. (c) Chetcuti, M. J. In *Comprehensive Organometallic Chemistry II*; Adams, R. D., Ed.; Pergamon Press: Oxford, U.K., 1995; Vol. 10. (d) Shriver, D. F., Kaesz, H., Adams, R. D., Eds. *The Chemistry of Metal Cluster Complexes*; VCH: New York, 1990. (e) Stephan, D. W. *Coord. Chem. Rev.* **1989**, *95*, 41−107.

(7) (a) Komiya, S.; Endo, I. *Chem. Lett.* **1988**, 1709−1712. (b) Miki, K.; Kasai, N.; Endo, I.; Komiya, S. *Bull. Chem. Soc. Jpn.* **1989**, *62*, 4033−4035. (c) Fukuoka, A.; Sadashima, T.; Sugiura, T.; Wu, X.; Mizuho, Y.; Komiya, S. *J. Organomet. Chem.* **1994**, *473*, 139−147. (d) Fukuoka, A.; Sadashima, T.; Endo, I.; Ohashi, N.; Kambara, Y.; Sugiura, T.; Miki, K.; Kasai, N.; Komiya, S. *Organometallics* **1994**, *13*, 4033−4044. (e) Fukuoka, A.; Sugiura, T.; Yasuda, T.; Taguchi, T.; Hirano, M.; Komiya, S. *Chem. Lett.* **1997**, 329−330. (f) Fukuoka, A.; Fukagawa, S.; Hirano, M.; Komiya, S. *Chem. Lett.* **1997**, 377−378. (g) Yasuda, T.; Fukuoka, A.; Hirano, M.; Komiya, S. *Chem. Lett.* **1998**, 29−30. (h) Komiya, S.; Muroi, S.; Furuya, M.; Hirano, M. *J. Am. Chem. Soc.* **2000**, *122*, 170−171.

(8) Due to the small size and low quality of the single crystals for **4**, the diffractometer could not collect enough reflection data (reflection/parameter ratio 3.0) even though the *R* value and GOF (*R* = 0.073, GOF = 1.87) were reasonable. Therefore, we have avoided detailed discussion concerning the bond distances and angles, except for the Pd−Co bond and the overall structure of **4**.

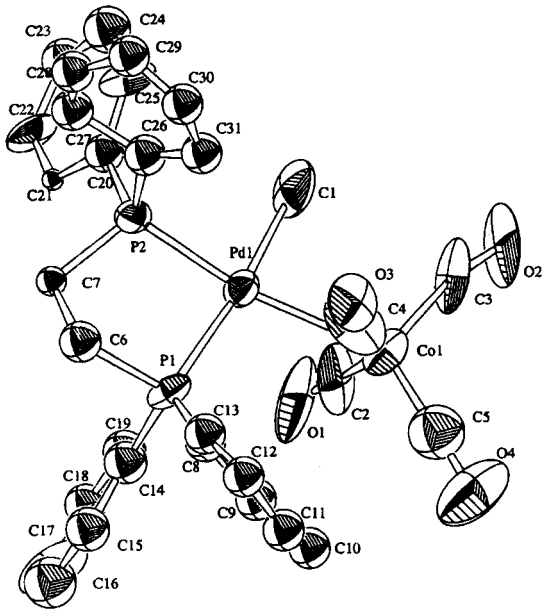

4

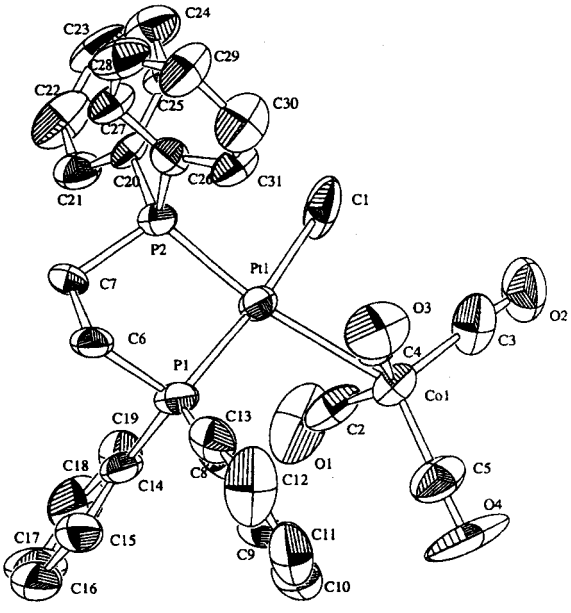

5

Figure 1. ORTEP drawings of (dppe)(CH_3)Pd−$Co(CO)_4$ (**4**) and (dppe)(CH_3)Pt−$Co(CO)_4$ (**5**).

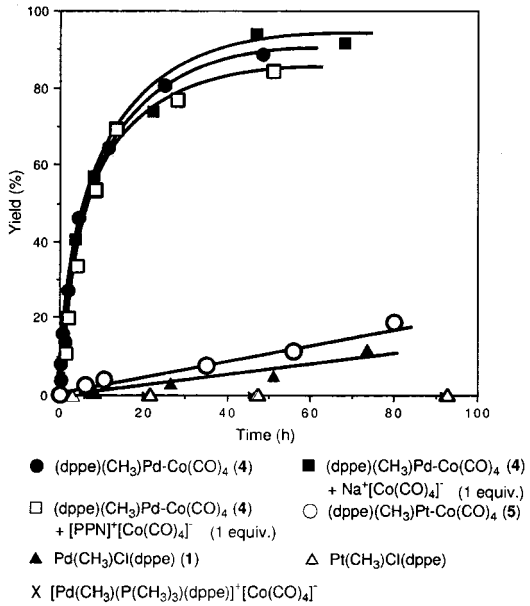

Figure 2. Time−yield curves of CO insertion.

Mo complex **2** gave the CO insertion product (dppe)-(CH_3C(O))Pd−$MoCp(CO)_3$ (22%) and the reductive elimination product $Mo(CH_3)Cp(CO)_3$ (27%). In contrast, no CO insertion took place for the Pd−W complex **3**, but $W(CH_3)Cp(CO)_3$ was quantitatively obtained from reductive elimination. For the Pt−Co complex **5**, the CO insertion proceeded at a slow rate to give (dppe)(CH_3C-(O))Pt−$Co(CO)_4$ (60%) in 10 days. From these results, it is shown that the presence of a $Co(CO)_4$ moiety provides good activity and selectivity of CO insertion to form the heterodinuclear acetyl complexes.

The reaction rates of CO insertion for several Pd−CH_3 and Pt−CH_3 complexes were monitored by NMR spectroscopy, employing samples of the complexes with concentrations of ca. 0.02 M in CD_2Cl_2 at 24 ± 1 °C and 1 atm (ca. 9-fold excess CO). Figure 2 represents time−yield curves of CO insertion to give the corresponding acetyl complexes. The Pd−Co complex **4** gave a significantly higher activity than the mononuclear Pd complex **1** and the Pt−Co complex **5** with methyl and dppe ligands; the initial rate of CO insertion for **4** was approximately 80 times faster than that of **1**. No CO insertion occurred for PtMeCl(dppe) under the same conditions. Hence, it is clearly shown that the CO insertion is enhanced by the $Co(CO)_4$ group over the Cl ligand for the methyl complexes of Pd and Pt with dppe ligands.

It is well-known that cationic Pd(II) complexes show a high activity of CO insertion. With this mechanism for the formation of **6** from **4** and CO, heterolytic cleavage of the Pd−Co bond may be possible to generate $[Pd(CH_3)(dppe)]^+[Co(CO)_4]^-$, and subsequent CO insertion on the Pd cation[9] and recombination of Pd−Co bond would provide **6**. In this case, addition of $[Co(CO)_4]^-$ would suppress the CO insertion. However, when 1 equiv of $Na^+[Co(CO)_4]^-$ or $[PPN]^+[Co(CO)_4]^-$ (PPN = $(Ph_3P)_2N$) was added to the reaction of **4** with CO, the time−yield curves were almost the same as that of **4** itself, as shown in Figure 2. Thus, the intermediacy of the cationic Pd(II) species is not likely to occur under our reaction conditions.[10] Accordingly, it is conceivable that the Pd−Co bond is retained in the CO insertion reaction.

Isotopic Labeling Experiment for CO Insertion. In the mechanism of the CO insertion on **4** to form **6**, the acetyl CO results from either gaseous CO or $Co(CO)_4$. Therefore, to reveal the origin of acetyl CO, isotopic labeling experiments were performed. When **4** was treated with ^{13}CO (27-fold excess, 99% ^{13}C-enriched) in benzene in a Schlenk tube at room temperature, a ^{13}C-enriched acetyl Pd−Co complex (**6***) was isolated in 82% yield in 6 h (eq 3). The ^{13}C content of the acetyl

(9) (a) Dekker, G. P. C. M.; Elsevier, C. J.; Vrieze, K.; van Leeuwen, P. W. N. M. *Organometallics* **1992**, *11*, 1598−1603. (b) Kayaki, Y.; Kawataka, F.; Shimizu, I.; Yamamoto, A. *Chem. Lett.* **1994**, 2171−2174. (c) Kayaki, Y.; Shimizu, I.; Yamamoto, A. *Chem. Lett.* **1995**, 1089−1090. (d) Markies, B. A.; Kruis, D.; Rietvelt, M. H. P.; Verkerk, K. A. N.; Boersma, J.; Kooijman, H.; Lakin, M. T.; Spek, A. L.; van Koten, G. *J. Am. Chem. Soc.* **1995**, *117*, 5263−5274.

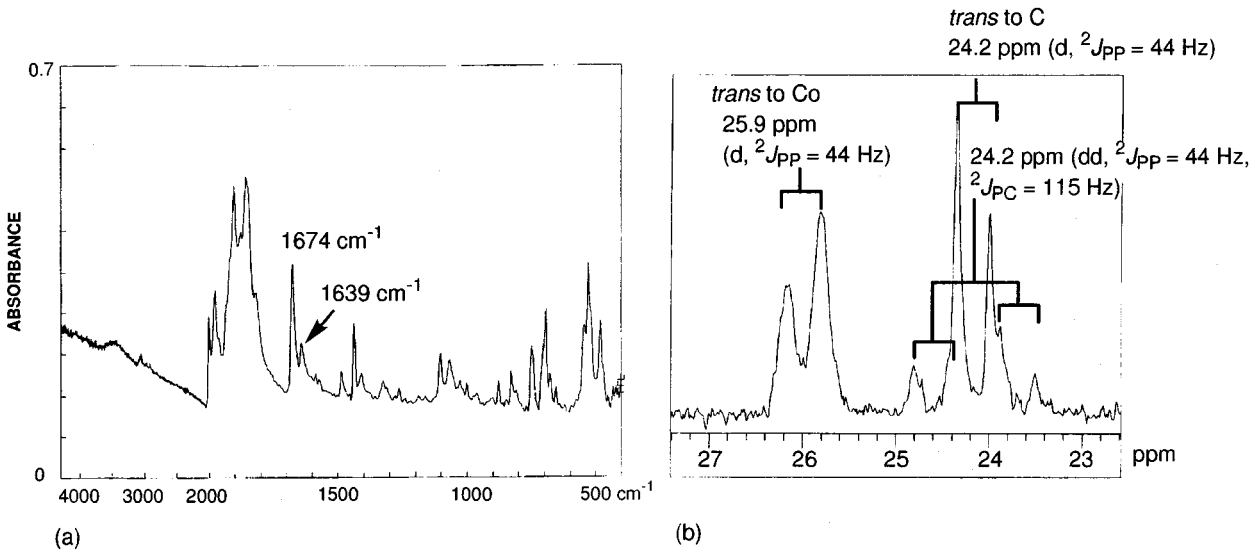

Figure 3. IR (a) and $^{31}P\{^1H\}$ NMR spectra (b) of ^{13}C-enriched (dppe)($CH_3C(O)$)Pd−$Co(CO)_4$ (**6***).

CO carbon was calculated by IR and $^{31}P\{^1H\}$ NMR spectroscopy. By comparison of the absorbance of acetyl groups ($\nu(^{12}CO)$ 1674 cm^{-1}, $\nu(^{13}CO)$ 1639 cm^{-1}) in the

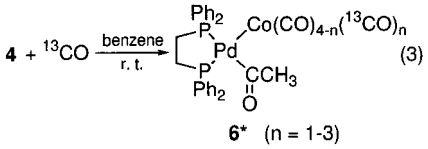

IR spectrum of **6***, the $^{12}C/^{13}C$ ratio was estimated to be 2.5 (Figure 3a). In the $^{13}C\{^1H\}$ NMR spectrum of **6***, the resonance due to $C(O)CH_3$ at δ 235.0 showed $^{31}P-^{13}C$ couplings ($^2J_{PC}$ = 12 and 115 Hz) with the phosphorus nuclei of dppe. On the other hand, in the $^{31}P\{^1H\}$ NMR spectrum of **6*** (Figure 3b), an AB pattern at δ 24.2 and 25.9 was observed as major species for the phosphorus nuclei trans to the acetyl and cobalt moieties, respectively, in which one doublet of doublets due to the $^{13}C-^{31}P$ ($^2J_{CP}$ = 115 Hz) and the $^{31}P-^{31}P$ ($^2J_{PP}$ = 44 Hz) couplings was also observed at 24.2 ppm as satellites. From the integral value of this peak, the $^{12}C/^{13}C$ ratio was estimated to be 2.0. Both the IR and $^{31}P\{^1H\}$ NMR data indicate that most of the acetyl carbonyl is ^{12}CO from $Co(CO)_4$. If ^{12}CO and ^{13}CO were statistically scrambled in the reaction mixture, the $^{12}C/^{13}C$ ratio would be 0.15 (4 ^{12}CO from $Co(CO)_4$ and 27 ^{13}CO from the gas phase). It is of great interest to note that the CO ligand in $Co(CO)_4$ preferentially inserts into the Pd−CH_3 bond even in the presence of 7-fold excess ^{13}CO in the gas phase. We infer that the minor $^{13}C(O)$-CH_3 species is formed by the direct attack of ^{13}CO at Pd or scrambling of gaseous ^{13}CO with the ^{12}CO ligand on $Co(CO)_4$, but the isotopic labeling experiments show that they are slower processes.

Theoretical Calculation for the Carbonyl Insertion Reaction into Pd−CH_3 Bond. To elucidate the reaction mechanism of the carbonyl insertion reaction into the Pd−CH_3 bond to form the acetyl group on the Pd atom, we performed B3LYP density functional calculations for the reaction (eq 4) of a model reactant, ($H_2PCH_2CH_2PH_2$)Pd(CH_3)−$Co(CO)_4$ (**7**), in which the phenyl groups of the bis-phosphine ligand are replaced by hydrogen atoms.

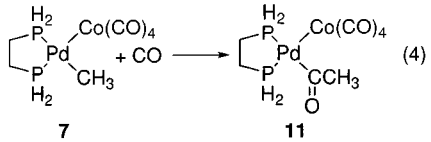

(a) Model Reactant ($H_2PCH_2CH_2PH_2$)Pd(CH_3)−$Co(CO)_4$. The optimized structure of the model reactant ($H_2PCH_2CH_2PH_2$)(CH_3)Pd−$Co(CO)_4$ (**7**), shown in Figure 4, is qualitatively in agreement with the X-ray structure of (dppe)(CH_3)Pd−$Co(CO)_4$ (**4**).[7f] For instance, the Pd−Co bond length in the experimental structure is 2.682(8) Å, whereas the calculated length is 2.643 Å.

To analyze the electronic structure of **7**, we localized the Kohn−Sham orbitals using the Boys algorithm.[11] The two orbitals representing the Pd−Co bond and the interaction between the Pd atom and the semibridging carbonyl groups are shown in Figure 5.[12] One can see in Figure 5a that there is a Pd d−Co d σ bond and that the bonding electrons delocalize into the π^* orbitals of the semibridging carbonyl ligands. As shown in Figure 5b, similar electron back-donation from the occupied Pd d orbitals to the π^* orbitals takes place as well.

Although one may ascribe the semibridging structure to this back-donation from the Pd atom, this is not the sole origin of semibridging. The structure of $CoH(CO)_4$

(10) Other mechanisms for the CO insertion on **4** are as follows. (1) dppe becomes monodentate and the semibridging CO migrates to Pd to result in CO insertion. To check this mechanism, we added 1 equiv of dppe or $P(CH_3)_3$ to **4**, but ionization took place to give the ionic complexes [(dppe)(CH_3)Pd(μ-dppe)Pd(CH_3)(dppe)]$^+$[$Co(CO)_4$]$^-$ and [Pd(CH_3)($P(CH_3)_3$)(dppe)]$^+$[$Co(CO)_4$]$^-$, respectively. Thus, it was difficult to prove this mechanism. However, we infer that the ionization to cationic Pd(II) species is a minor process, because (dppe)($CH_3{}^{13}C$-(O))Pd−$Co(CO)_4$ was a minor product in the reaction of **4** with ^{13}CO (vide infra). [Pd(CH_3)($P(CH_3)_3$)(dppe)]$^+$[$Co(CO)_4$]$^-$ showed no activity of CO insertion under the conditions of Figure 2. (2) CO enhances the reductive elimination of $Co(CH_3)(CO)_4$ from **4** to give "Pd(dppe)" species, and CO insertion and coordination of CO provide $Co(C(O)CH_3)(CO)_4$. Oxidative addition of the acetyl Co complex to "Pd(dppe)" gives (dppe)-($CH_3C(O)$)Pd−$Co(CO)_4$. This is still a possible way to explain the results of the ^{13}CO labeling experiment.

(11) (a) Boys, S. F. *Rev. Mod. Phys.* **1960**, *32*, 296−299. (b) Foster, J. M.; Boys, S. F. *Rev. Mod. Phys.* **1960**, *32*, 300−302.

(12) The localized orbitals obtained from the RHF orbitals are qualitatively the same as those based on the Kohn−Sham orbitals.

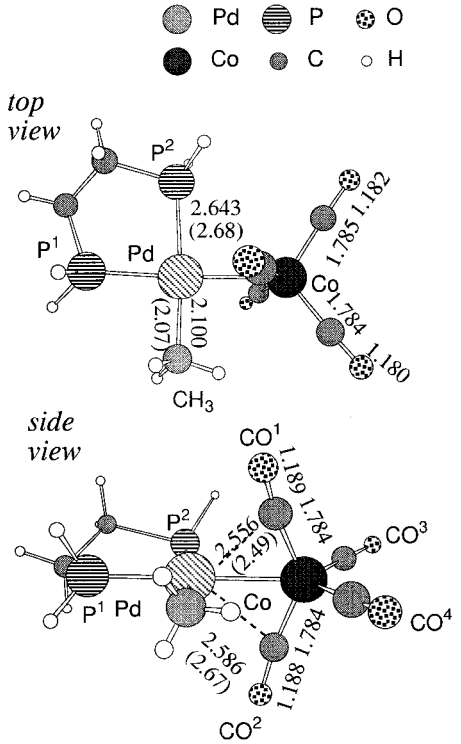

Figure 4. Optimized structure of $(H_2PCH_2CH_2PH_2)(CH_3)$-Pd−Co$(CO)_4$ (**7**), with bond distances in Å. The experimental bond distances are in parentheses.

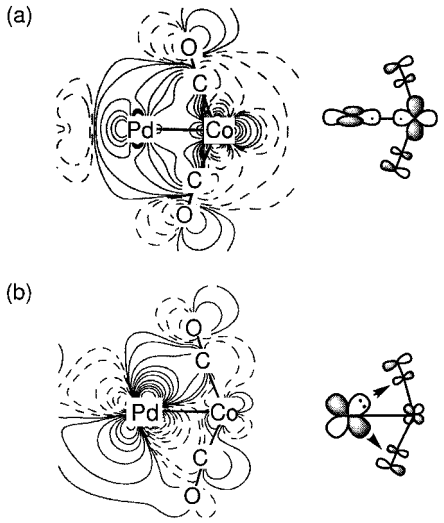

Figure 5. Localized orbitals representing (a) the Pd−Co bond and (b) donation from the occupied Pd d orbital to CO π^* orbitals.

has been studied theoretically[13] to show that, although it is not an equilibrium structure, $CoH(CO)_4$ with an equatorial hydride (C_{2v} symmetry) displays bending of CO ligands toward the H ligand.[14] The calculations at the present level gave an H−Co−CO^{ax} angle of 73.0° in $CoH(CO)_4$, as shown in Chart 1 , and also gave C−Co−CO^{ax} angles of 78.5 and 78.5−78.7° in $Co(CH_3)(CO)_4$ and $Co(CH(CH_3)_2)(CO)_4$, respectively. These results show that CO bending is normal for tetracarbonylcobalt complexes with an equatorial σ bond and that back-donation in **7** plays a secondary role to reduce the angles to 67−68°.

Chart 1

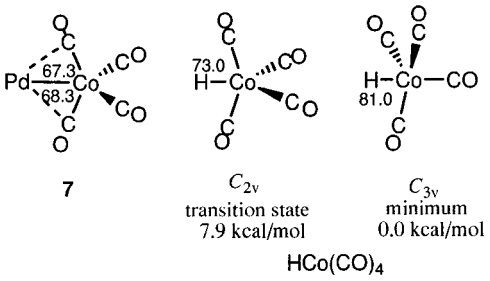

Scheme 1

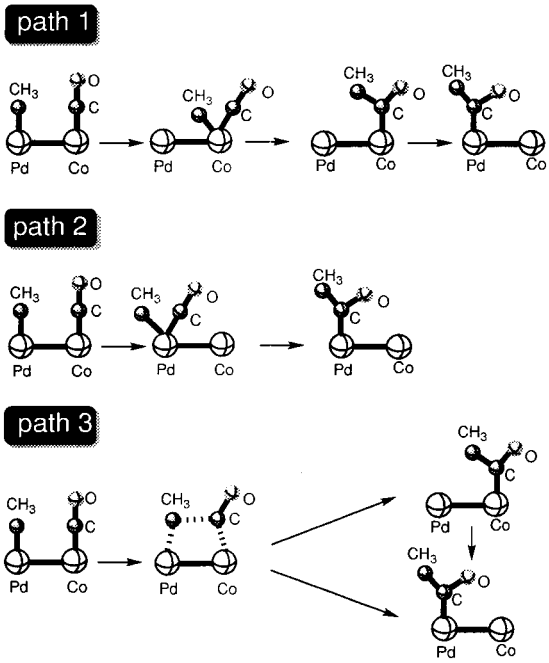

However, electron-back-donation plays an energetically important role. The C_{2v} structure of $CoH(CO)_4$ with an equatorial Co−H σ bond is not an equilibrium structure but a transition state connecting the two C_{3v} equilibrium structures, which are 7.9 kcal/mol more stable than the C_{2v} structure. This indicates that the structure of the Co moiety with an equatorial Pd−Co σ bond is an equilibrium structure due to back-donation in **7**.

Starting from **7**, there are three possible reaction paths shown in Scheme 1. In path 1 the methyl group on the Pd atom migrates to the Co atom so that the carbonyl insertion takes place on the Co atom. Finally the acetyl group migrates from the Co atom to the Pd atom to lead to the product. In path 2 one of the carbonyl groups on the Co atom migrates to the Pd atom and then the carbonyl insertion takes place on the Pd atom. In path 3 the CC bond is directly formed between the two groups on the two metals. We have theoretically studied these three reaction paths. We performed theoretical calculations at the B3LYP density functional level using set I for structure determinations and the basis set II for final energy calculations. In the following discussions we will refer to the energies calculated at the B3LYP/II//B3LYP/I level, unless otherwise mentioned.

(b) Reaction Starting with the Methyl Migration from Pd to Co: Path 1.

(13) Torrent, M.; Sola, M.; Frenking, G. *Chem. Rev.* **2000**, 439−493.
(14) (a) Elian, M.; Hoffmann, R. *Inorg. Chem.* **1975**, *14*, 1058−1076. (b) Versluis, L.; Ziegler, T.; Baerends, E. J.; Ravenek, W. *J. Am. Chem. Soc.* **1989**, *111*, 2018−2025.

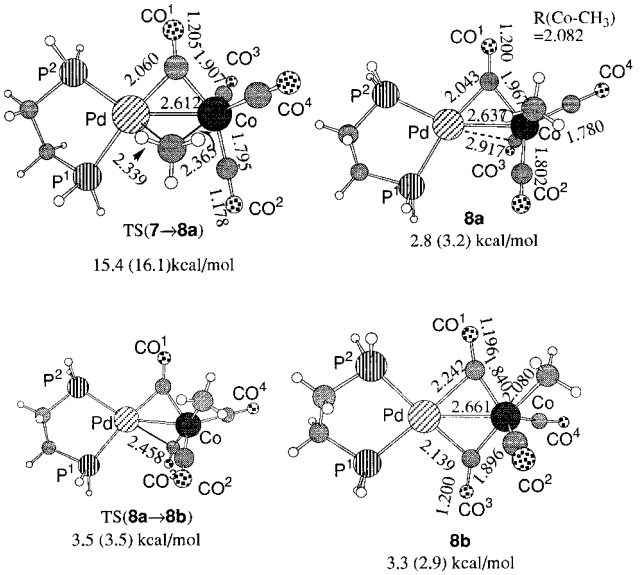

Figure 6. Optimized structures of the transition state and product for methyl migration in path 1. Energies are relative to **7** in kcal/mol at the B3LYP/II(B3LYP/I) level.

Chart 2

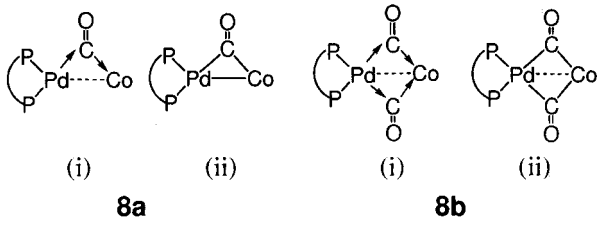

The first step of path 1 is methyl migration from the Pd atom to the Co atom. The optimized structures for this step are shown in Figure 6. The methyl migration passes through the transition state, TS(**7**→**8a**), with an activation energy of 15.4 kcal/mol. At TS(**7**→**8a**) the methyl group bridges the two metal atoms, as expected for migration reactions, with Pd−CH_3 and Co−CH_3 distances of 2.339 and 2.365 Å, respectively. Also, one of the CO groups (CO^1) bridges the two metal atoms. The product of this step is intermediate **8a**, in which the migrating methyl group occupies the axial position of the Co moiety with a deformed trigonal-bipyramidal (TBP) structure, a structure favorable for d^8 five-coordinate complexes such as $CoH(CO)_4$ mentioned above. In **8a** CO^1 continues to bridge the metal atoms. There is another isomeric structure with the two CO bridges, **8b,** shown in Figure 6. The isomerization from **8a** to **8b**, which includes the rotation of the TBP Co moiety and results in bond formation between the Pd atom and the CO^3 carbon atom, is 0.5 kcal/mol endothermic, and its activation energy is only 0.7 kcal/mol. These small values indicate that the potential energy surface in this region is quite flat and that fluxional behavior is expected.

For **8** with CO bridge(s) we have two possible ways of drawing chemical bonds, as shown in Chart 2. (i) The electron donation from Pd d orbital to the π^* orbital of the bridging CO groups is responsible for the bonding interaction between two fragments in addition to the bonds between the metal atoms, shown by broken lines. (ii) On the other hand, the bridging CO groups are ketonic. The Pd and Co atoms in (i) have d^{10} and d^8 formal electron configurations, respectively, whereas those in (ii) have d^8 and d^6 configurations, respectively.

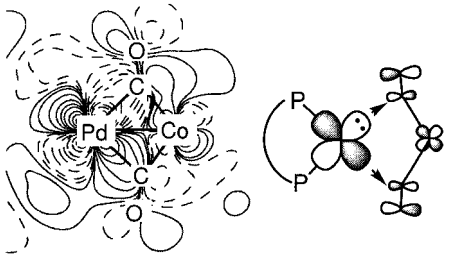

Figure 7. Localized orbitals for electron back-donation from the occupied Pd d orbital to the CO π^* orbitals in **8b**.

To know which is a better model, we again calculated localized orbitals to find that the first model properly represents the interaction between the two fragments. For instance, the localized orbitals shown in Figure 7 demonstrates the electron donation from the occupied Pd d orbital to the π^* orbitals of the bridging CO groups in **8b**, whereas we did not obtain a localized orbital representing a Pd−Co σ bond. d^{10} ML_2 complexes with an L−M−L angle of about 90° like the Pd fragment in **8a** and **8b** have an unstable occupied d orbital which is known to activate even CH bonds. The electron back-donation to the π^* orbitals stabilizes such an unstable Pd fragment. This is an energetically important factor of the reaction, and stabilization due to this electron back-donation is observed in other intermediates and TSs in the present path.

In the second step of path 1 the bond between the methyl group on the Co atom and one of the CO groups is formed. The methyl group in **8a** and **8b** can react with bridging or terminal CO groups. The structures for three reaction paths, one from **8a** and two from **8b**, are shown in Figure 8. The reaction with terminal CO^2 in **8b**, which gives **9b**, is just a migratory carbonyl insertion into the Co−CH_3 bond. During the course of this reaction the carbonyl group does not insert into the bond, but the methyl group migrates to the CO^2 group. This reaction passes through three-centered TS(**8b**→**9b**) with an activation energy of 8.9 kcal/mol. While the H_3C-CO^2 bond distance is 1.954 Å, which is 1.25 times longer than that of 1.559 Å in the product, the Co−CH_3 bond of 2.248 Å is only 1.081 times longer compared with that of 2.080 Å in **8b**. While the H_3C-CO^2 bond is partially formed, the Co−CH_3 bond is hardly stretched. Asynchronous bond exchange like this has been theoretically found in the TSs for various CO migratory insertions.[15] The local structure of the Co fragment of this TS is square pyramidal with the apical CO^4 group, and the bond exchange takes place in the basal plane. The reaction with another terminal CO group, CO^4, is expected to be similar, and therefore we did not investigate this reaction.

The reaction of the methyl group with the bridging carbonyl group, CO^1, in **8b** was shown to take place with an activation energy of 8.3 kcal/mol, only 0.6 kcal/mol smaller than that for the reaction with the terminal CO^2 group. Also, the H_3C-CO^1 bond distance of 1.925 Å and the Co−CH_3 bond distance of 2.238 Å in the transition state, TS(**8b**→**9a**), with a square-pyramidal structure of the Co moiety, are similar to those in TS(**8b**→**9b**). At

(15) Koga, N.; Morokuma, K. *Chem. Rev.* **1991**, *91*, 823−842.

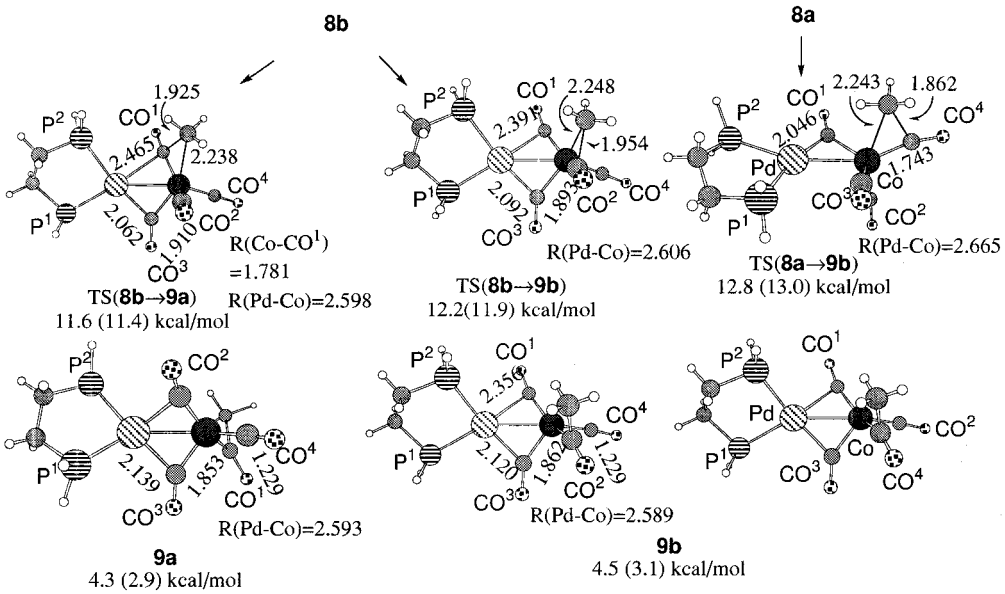

Figure 8. Optimized structures for CO insertion reactions from **8a** and **8b**. The bond distances and angles are given in Å and deg, respectively. The energies are relative to **7** at the B3LYP/II(B3LYP/I) level.

this TS the Pd−CO^1 bond is stretched by 0.22 Å, and the $CoCO^1$ fragment is more linear compared with that in **8b**. These results show that the CO^1 group at TS(**8b→9a**) is similar to the terminal carbonyl in character. In a comparison between **8a** and **8b**, one notices that the second CO bridging easily breaks. Accordingly, it is not surprising that these two reactions are energetically similar. During the course of the reaction from **8b** to **9a** the Co fragment rotates so that CO^2 bridges the metal atoms in **9a**, suggesting that the acetyl group is not sufficiently electron-accepting to form bridges. **9a** and **9b** are enantiomeric, except for the conformation of the ethylene bridge in the bis-phosphine ligand. Therefore, these two intermediates are isoenegetic. In **9a** and **9b** the agostic interaction between the β-C−H bond of the acetyl ligand and the Co atom takes place as shown by the short Co−H^β distance of 2.383 and 2.379 Å in **9a** and **9b**, respectively.

We can consider three reaction pathways from **8a** as well. However, we found only one transition state structure, TS(**8a→9b**). In several trials for finding other transition states we obtained only TS(**8b→9a**) and TS(**8b→9b**), showing that at the TSs CO bridging is newly formed to stabilize the reaction system. On the other hand, in the reaction **8a→9b**, CO^3 bridges the metal atoms after passing through TS(**8a→9b**). The activation energies for all these CO insertion reactions are similar, 8.3−10.0 kcal/mol, and thus we can say at the present level of calculations that all the insertion reactions are possible. Since these reactions are on the single metal atom, the profile of the reactions is expected to be similar to that for the reaction of mononuclear complexes. As a matter of fact, the calculations for the carbonyl insertion reaction of $Co(CH_3)(CO)_4$ at the same level of calculations showed that the mononuclear reaction requires an activation energy of 10.8 kcal/mol, to show that the Pd fragment has a small electronic effect on the activation energy. The TS for the reaction of $Co(CH_3)(CO)_4$ has a square-pyramidal framework, and the product has an agostic acyl ligand with a Co−H^b distance of 2.272 Å.[16] They are the same geometrical features as found in the TSs of the Pd−Co complex.

The bond formation in the migratory CO insertion takes place on the Co atom, and thus the resultant acetyl group has to migrate to the Pd atom. In addition, the extra CO group has to coordinate to the Co atom, to lead to the final product. Therefore, there are two possibilities for reaction paths. In one path (path a), first CO coordinates to the Co atom followed by acetyl migration, and in another path (path b) acetyl migration prior to CO coordination takes place.

Concerned with path a, as shown in Figure 9, we found the transition state TS(**10b→11**) for the acetyl migration. The reactant corresponding to this TS is **10b**, in which the Co moiety has a deformed TBP structure and one of the CO groups bridges the metal atoms. At the B3LYP/I level we found another equilibrium structure, **10a**, with the two CO bridges. This is considered to be the intermediate formed by CO coordination to **9**, and it is 18.7 kcal/mol more stable than **9a** + CO. CO groups in **10a** are numbered by assuming that the fifth CO group coordinates to the Co atom between CO^2 and the acetyl groups of **9a**. There is a transition state between **10a** and **10b**, TS(**10a→10b**), at the B3LYP/I level. However, at the B3LYP/II//B3LYP/I level TS(**10a→10b**) is more stable than **10a**, indicating that **10a** does not exist as an equilibrium structure and that CO coordination to **9** directly results in the structure with a single CO bridge, **10b**. Also, the small energy difference between **10a** and **10b** suggests that, similar to the case of **8a** and **8b**, the potential energy surface is flat and the structure is fluxional. During the process from **10b** to TS(**10b→11**) the Co moiety rotates around the Co−CO^3 bond so that the migrating acetyl group bridges the metal atoms. While the reaction from **10b** is 7.3 kcal/

(16) In the case of $Co(C(O)CH_3)(CO)_4$ the structure with a Co−O interaction is more stable than that with an agostic interaction. This is true in the Pd−Co complex. The structure with the Co−O interaction is 4 kcal/mol more stable than **9a**. However, the transition state for the acetyl migration is not connected to it, and therefore we omitted it in discussions.

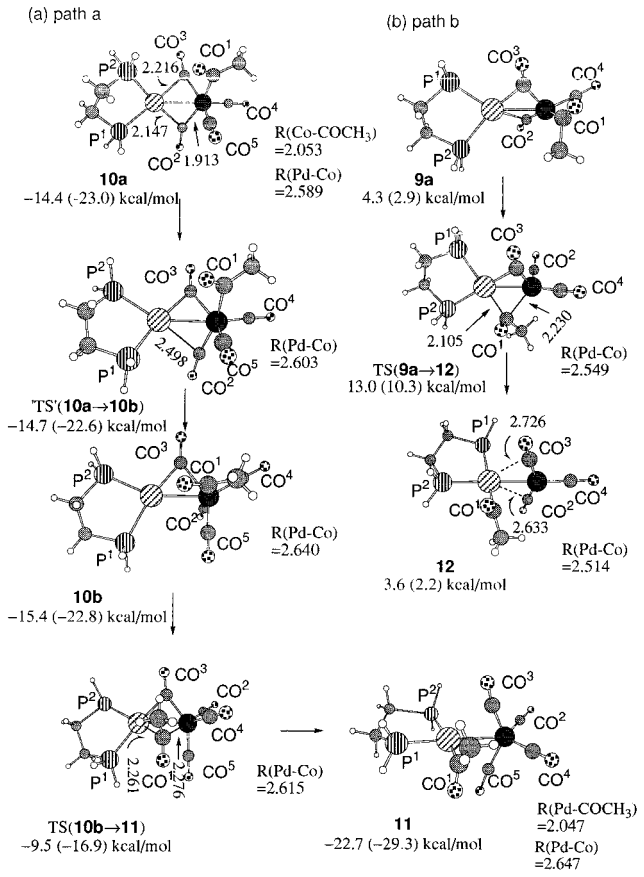

Figure 9. Optimized structures for acetyl migration from the Co atom to the Pd atom. In path a the migration follows the CO coordination, and in path b the acetyl migration first takes place in **9a**. The energies are relative to **7** + CO for the reactions from **10a** and relative to **7** for the reactions from **9a** at the B3LYP/II(B3LYP/I) level.

mol exothermic, the activation energy for the acetyl group migration from **10b** was calculated to be 5.9 kcal/mol. In the final product **11** the two carbonyl groups semibridge the metal atoms as in the reactant, **7**. This acetyl group migration from the Co atom to the Pd atom is analogous to the reverse reaction, **8a**→**7**, of the methyl migration. The distances of the $COCH_3$ group from the metal atoms in TS(**10b**→**11**) are shorter than those of the CH_3 group in TS(**7**→**8a**), suggesting that the CO π orbitals of the acetyl group interact with the metal d orbitals to stabilize the transition state. The smaller activation energy for **11**→**10b** than that for **7**→**8a** is consistent with this.

If the acetyl group migration takes place prior to the CO coordination, the reaction passes through TS(**9a**→**12**), shown in Figure 9. While the acetyl group in TS(**9a**→**12**) bridges the two metal atoms as in TS(**10b**→**11**), the reaction from **9a** to **12** requires 3 kcal/mol greater activation energy, being less favorable than the reaction from **10b** to **11**. Different from the exothermic reaction **10b**→**11**, the reaction **9a**→**12** is almost thermoneutral. This is presumably because this reaction gives a coordinatively unsaturated Co fragment. In the last stage of path b CO coordination takes place with an exothermicity of 26 kcal/mol to lead to the final product.

(c) Comparison of Path 1 with the Other Paths. We extensively searched transition states for the CO migration in path 2 from the Co atom to the Pd atom to find only one transition state in which the P^2 atom almost dissociates from the Pd atom and CO^3 migrates to the vacant site thus generated. The activation energy of this CO migration (21 kcal/mol) is larger than that of the methyl migration of path 1 and thus less favorable. In the present system the five-coordinated Pd fragment is too unstable to exist. Similarly, during the structure determination of $(OC)(H_2PCH_2CH_2PH_2)(CH_3)$-$Pd-Co(CO)_4$, one of the P atoms dissociates. The activation barrier to the direct C−C bond formation between the CH_3 group on the Pd atom and the CO ligand on the Co atom in path 3 was calculated to be 25 kcal/mol, which is the largest. In addition, during the course of the reaction one of the P atoms migrates to the Co atom. It is unlikely that such an elementary step is the part of the present reaction. Consequently, we can conclude that path 1 is the reaction path for the acetyl group formation in the Pd−Co complex.

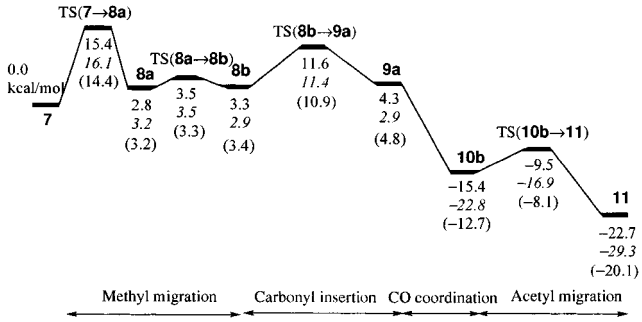

Figure 10. Energy profile for the favorable path for reaction 4 calculated at the B3LYP/II//B3LYP/I level. Enthalpies in italics are those at the B3LYP/I//B3LYP/I level, and enthalpies in parentheses are those calculated at 298.15 K.

(d) Energy Profile. The profile of potential energy as well as enthalpy calculated at 298.15 K for the favorable reaction path is summarized in Figure 10. As for the CO migratory insertion there are several comparable reaction paths, and the profile for **8b**→**9a** was adopted in Figure 10. The first step of the methyl migration is rate-determining, which requires an activation energy of 15.4 kcal/mol. The CO insertion on the Co atom and the following acetyl migration are easier. The effects of basis set are small for the intramolecular migration and insertion reactions, whereas those for the CO coordination is not negligible. Because of the basis set superposition error the CO binding energy is overestimated using the basis set I. The larger basis set II improves the energetics. Thermal contributions taken into account in enthalpy do not change the profile qualitatively.

In the present reaction, the Co fragment is chosen as the site for the C−C bond formation, and the methyl group migration between the two metal centers is a key reaction. The important factor which realizes the methyl migration is electron back-donation from the Pd occupied orbital to the CO π^* orbitals as discussed above, which stabilizes the unstable d^{10} Pd fragment. Accordingly, a similar migration could take place in complexes with late-transition-metal atoms such as Pd. Though of lower reactivity, the same reaction is experimentally known for the Pt−Co analogue as mentioned above. Our B3LYP/I calculations showed that the methyl migration

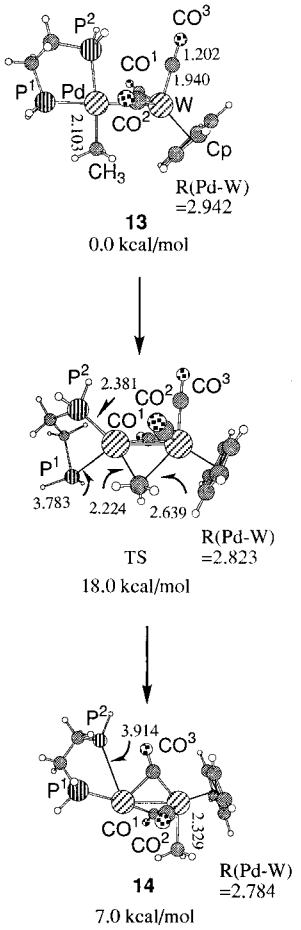

Figure 11. Optimized structures for methyl migration in $(H_2PCH_2CH_2PH_2)(CH_3)Pd-WCp(CO)_3$, (**13**). The distances and angles are given in Å and deg, respectively. The energies are relative to **13**.

(eq 5) is possible, but the activation barrier (24.3 kcal/mol) is 9 kcal/mol larger than that of the Pd−Co system

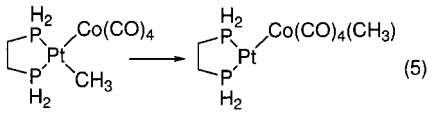

(5)

in agreement with the experimental observation. The stronger Pt−C bond results in a greater activation energy.

(e) Comparison of Methyl Migration with That of the Pd−W Complex. These results suggest that the situation could be different in heterodinuclear complexes with earlier transition metals. The heterodinuclear Pd−W complex similar to the present reactant is experimentally known, in which the methyl group is on the Pd atom and three carbonyl groups are on the W atom.[17] As mentioned above, the heterodinuclear Pd−W complex **3** does not conduct CO insertion. Thus, to elucidate the origin of the difference, we studied similar model methyl migration for $(H_2PCH_2CH_2PH_2)(CH_3)Pd-WCp(CO)_3$ (**13**), as shown in Figure 11. The activation energy was calculated to be 18 kcal/mol, not much higher than that for the Pd−Co system and smaller than that for the Pt−Co system. However, the difference is found in the structure of the bis-phosphine fragment in the TS as well as in the product. The P^2 atom dissociates, the corresponding $Pd-P^2$ distance at the TS and product being 3.783 and 3.914 Å, respectively. The earlier, more electropositive W atom donates its d electrons into the π^* orbitals of CO more than the Co atom.[18] Because of this stronger back-donation the carbonyl C−O distances of 1.20 Å in the Pd−W complex are longer than those in **7**. Electron-rich CO groups on the W atom cannot stabilize the Pd fragment by accepting electrons from the Pd atom, and therefore, to avoid the unstable structure of the Pd fragment the phosphorus atom dissociates.

The interaction between the Pd and W fragments in **14** should be weaker than that between the Pd and Co fragments. Actually the interaction between the two metal fragments in **14** was calculated to be weaker by 8−9 kcal/mol, as shown in eqs 6 and 7, and the

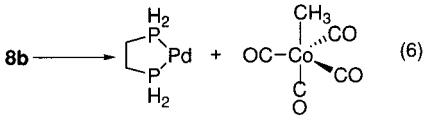

(6)

ΔE = 24.3 kcal/mol
ΔG = 12.2 kcal/mol (298.15 K)

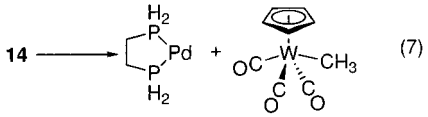

(7)

ΔE = 15.1 kcal/mol
ΔG = 4.4 kcal/mol (298.15 K)

dissociation into Pd and W fragments is possible, different from the Pd−Co system. This result shows that the present reaction depends on the nature of the transition metals and accounts for the experimental observation that $W(CH_3)Cp(CO)_3$ was obtained from reductive elimination.

Concluding Remarks

We have studied the cooperative effects in the Pd−Co, Pd−Mo, and Pd−W heterodinuclear complexes. The treatment of **4** with ^{13}CO resulted in the preferential insertion of the carbonyl on Co into the Pd−C bond and the incoming CO locates on Co. The B3LYP hybrid density functional calculations suggest that this insertion reaction proceeds via methyl migration from Pd to Co, insertion of a carbonyl into the CH_3-Co bond, coordination of incoming carbon monoxide to the vacant site in Co, and migration of the acetyl group from Co to Pd, which is in good agreement with the experimental results. Such facile migration of the organic group depends on the nature of the transition-metal fragment. In the Pd−W system the activation energy for the methyl migration is as much as that in the Pd−Co system. However, the more electron rich W fragment dispenses its electrons to back-donation to the carbonyl

(17) Komiya, S. Unpublished results. Reaction of $Pd(CH_3)Cl(cod)$ with $Na^+[WCp(CO)_3]^-$ also gave $(cod)(CH_3)Pd-WCp(CO)_3$, which slowly afforded $W(CH_3)Cp(CO)_3$ during the purification process. The Pt analogue $(cod)(CH_3)Pt-WCp(CO)_3$ reacted with CO, giving $W(CH_3)Cp(CO)_3$ in good yield, but no insertion product was obtained.[7d]

(18) (a) Pauling electronegativities for Co and W are 1.8 and 1.7, respectively. Pauling, L. *The Nature of the Chemical Bond*; Cornell University Press: Ithaca, NY, 1960. (b) Orbital energies (in au) for neutral W and Co atoms are as follows: W, 5d (−0.45), 6s (−0.22); Co, 3d (−0.68), 4s (−0.27). Fraga, S.; Karwowski, J.; Saxena; K. M. S. *Handbook of Atomic Data*; Elsevier: Amsterdam, 1976.

groups and cannot stabilize the Pd−W bond, leading to a simple alkyl transfer reaction. These results will provide a fundamental understanding of the synergistic effect of the related bimetallic catalysis.

Experimental Section

All manipulations were carried out under an atmosphere of nitrogen or argon using standard Schlenk techniques.[1b,19] Solvents were dried over and distilled from appropriate drying agents under N_2: hexane, benzene, toluene, diethyl ether, and THF from Na/benzophenone ketyl; CH_2Cl_2 from P_2O_5. NMR solvents were freeze−pump−thaw-degassed and vacuum-transferred from appropriate drying agents (C_6D_6 from Na; $CDCl_3$ and CD_2Cl_2 from P_2O_5). 1,2-Bis(diphenylphosphino)-ethane (dppe) was prepared by the literature method.[20] $[PPN]^+Cl^-$ (PPN = $(Ph_3P)_2N$), CO (99.9%), and ^{13}CO (99%) were used as received. IR spectra were measured on a JASCO FT-IR 5M spectrometer. NMR spectra were obtained on a JEOL FX-200 (^1H, 199.5 MHz) or a JEOL LA-300 (^1H 300.4 MHz) spectrometer. Chemical shifts were relative to $Si(CH_3)_4$ (^1H and ^{13}C) and 85% H_3PO_4 (^{31}P). Elemental analyses were performed with a Perkin-Elmer 2400 series II CHN analyzer. Molar electric conductivity was measured on a TOA CM-7B conductimeter.

The starting materials and related complexes were prepared by the literature methods with minor modifications: $Pd(CH_3)$-Cl(cod),[21] $Pt(CH_3)Cl(dppe)$,[22] $Pt(CH_2CH_3)Cl(dppe)$,[23] $Na^+[MoCp$-$(CO)_3]^-$,[24] $Na^+[WCp(CO)_3]^-$,[25] $Na^+[Co(CO)_4]^-$,[25] and $[PPN]^+[Co$-$(CO)_4]^-$.[26] $Pd(CH_3)Cl(dppe)$ was prepared by the ligand substitution reaction of $Pd(CH_3)Cl(cod)$ with an equimolar amount of dppe in benzene at room temperature. The precipitated white powder was washed with hexane, and recrystallization from a mixture of CH_2Cl_2 and hexane gave white crystals (yield 98%).

Synthesis of Heterodinuclear Complexes. A typical procedure for $(dppe)(CH_3)Pd-Co(CO)_4$ (**4**) is given. To a THF solution of $Pd(CH_3)Cl(dppe)$ (460.8 mg, 0.830 mmol) was added $AgNO_3$ (141.7 mg, 0.834 mmol). Stirring at room temperature gave a colorless solution with a white precipitate of AgCl. To the filtered solution was added a THF solution of $Na^+[Co(CO)_4]^-$ (182.4 mg, 0.926 mmol) at −20 °C, and the mixture was stirred for 2 h. The reaction mixture was evaporated to dryness, and the resulting solid was extracted with benzene. Addition of hexane to the concentrated solution of extracts gave red cubes. The crystals were washed with cold hexane and dried under vacuum (369.1 mg, 0.534 mmol). Yield: 64%. Mp: 123 °C dec. Anal. Calcd for $C_{31}H_{27}O_4P_2CoPd$: C, 53.90; H, 3.94. Found: C, 53.98; H 3.96. Molar electric conductivity Λ (THF, 24 °C): 0.017 S cm^2 mol^{-1}. IR (ν(CO), KBr): 2020, 1953, 1913, 1885 cm^{-1}. ^1H NMR (C_6D_6): δ 1.21 (dd, $^3J_{PH}$ = 7.7, 5.0 Hz, 3H, CH_3), 1.6−1.9 (m, 4H, dppe CH_2), 7.0−7.6 (m, 20H, dppe C_6H_5). $^{31}P\{^1H\}$ NMR (C_6D_6): δ 37.2 (d, $^2J_{PP}$ = 26 Hz), 49.4 (d, $^2J_{PP}$ = 26 Hz). $^{13}C\{^1H\}$ NMR (C_6D_6): δ 9.8 (d, $^2J_{PC}$ = 106 Hz, CH_3), 27.8 (dd, J_{PC} = 24, 16 Hz, dppe CH_2), 29.2 (dd, J_{PC} = 26, 22 Hz, dppe CH_2), 129−134 (m, dppe C_6H_5), 210 (br s, CO).

$(dppe)(CH_3)Pd-MoCp(CO)_3$ (2). This compound was obtained as yellow-brown needles from a mixture of toluene and hexane. Yield: 38%. Mp: 122 °C dec. Anal. Calcd for $C_{35}H_{32}O_3P_2MoPd$: C, 54.96; H, 4.22. Found: C, 55.35; H 4.48. Λ (THF, 24 °C): 0.0069 S cm^2 mol^{-1}. IR (ν_{CO}, KBr): 1901, 1792 cm^{-1}. ^1H NMR (C_6D_6): δ 1.52 (dd, $^3J_{PH}$ = 6.0, 7.8 Hz, 3H, CH_3), 1.7−1.8 (m, 4H, dppe CH_2), 4.69 (s, 5H, Cp), 7.0−7.8 (m, dppe C_6H_5). $^{31}P\{^1H\}$ NMR (C_6D_6): δ 35.4 (d, $^2J_{PP}$ = 18 Hz), 56.8 (d, $^2J_{PP}$ = 18 Hz).

$(dppe)(CH_3)Pd-WCp(CO)_3$ (3). This compound was obtained as yellow-brown needles from toluene/hexane. Yield: 29%. Mp: 108 °C dec. Λ (THF, 24 °C): 0.0038 S cm^2 mol^{-1}. This complex was identified by spectroscopic methods. IR (ν(CO), KBr): 1893, 1785 cm^{-1}. ^1H NMR (C_6D_6): δ 1.69 (t, $^3J_{PH}$ = 6.9 Hz, 3H, CH_3), 1.6−1.7 (m, 4H, dppe CH_2), 4.64 (s, 5H, Cp), 6.9−7.8 (m, 20H, dppe C_6H_5). $^{31}P\{^1H\}$ NMR (C_6D_6): δ 38.2 (d, $^2J_{PP}$ = 18 Hz), 60.7 (d, $^2J_{PP}$ = 18 Hz).

The dinuclear ethyl complexes $(dppe)(CH_3CH_2)Pt-ML_n$ (ML_n = $MoCp(CO)_3$, $WCp(CO)_3$, and $Co(CO)_4$) were prepared according to the procedures reported previously.[7e]

X-ray Structure Analyses. A Rigaku four-circle diffractometer with graphite-monochromatized Mo Kα radiation (0.710 69 Å) was used for data collection. The unit cells were determined by the automatic indexing of 25 centered reflections. Data were measured via ω-scans and corrected for Lorentz and polarization effects. The structures were solved and refined using the TEXSAN program system (Rigaku).

Complex 4. A selected single crystal with dimensions 0.19 × 0.19 × 0.06 mm was mounted in a thin glass capillary (GLASS 0.7 mmf) under N_2. Reflection data were collected at 296 K, and out of 7052 unique reflections, 904 ($|F_o| > 3\sigma|F_o|$) were observed. The structure was solved by Patterson methods and refined by a full-matrix least-squares procedure. All the non-hydrogen atoms except C3, C7, C14−C16, C19−C21, and C23−C24 were refined anisotropically. Hydrogen atoms were included in the calculation, but they were not refined. Crystallographic data for **4**: $C_{31}H_{27}O_4P_2CoPd$, fw = 690.83, monoclinic, $P2_1/n$ (No. 14), red, a = 10.782(8) Å, b = 17.681(6) Å, c = 15.950(7) Å, β = 103.59(4)°, V = 2955(2) Å^3, T = 296 K, Z = 4, R (R_w) = 0.073 (0.045), GOF = 1.87.

Complex 5. A selected single crystal with dimensions 0.50 × 0.41 × 0.16 mm was mounted in a thin glass capillary (GLASS 0.7 mmf) under N_2. Reflection data were collected at 296 K, and out of 5421 unique reflections, 2709 ($|F_o| > 3\sigma|F_o|$) were observed. The structure was solved by direct methods and refined by a full-matrix least-squares procedure. All the non-hydrogen atoms were refined anisotropically. Hydrogen atoms were included in the calculation, but they were not refined. Crystallographic data for **5**: $C_{31}H_{27}O_4P_2CoPt$, fw = 779.52, monoclinic, $P2_1/n$ (No. 14), orange, a = 10.741(6) Å, b = 17.716(7) Å, c = 15.982(5) Å, β = 103.56(3)°, V = 2956(2) Å^3, T = 296 K, Z = 4, R (R_w) = 0.049 (0.038), GOF = 1.81.

Synthesis of Acyl Complexes by CO Insertion. A typical preparative procedure for $(dppe)(CH_3C(O))Pd-Co(CO)_4$ (**6**) is given. **4** (97.3 mg, 0.141 mmol) was dissolved in benzene under N_2, and the solution was degassed in a Schlenk tube. CO (1 atm) was introduced into the Schlenk tube, and the orange solution turned to red after stirring for 16 h. The mixture was filtered, and the filtered solution was evaporated to dryness. The resulting solids were extracted with benzene, and addition of hexane to the concentrated solution of extracts gave yellow needles. The crystals were washed with cold hexane and dried under vacuum (86.4 mg, 0.120 mmol). Yield: 85%. Mp: 118 °C dec. Anal. Calcd for $C_{32}H_{27}O_5P_2CoPd$: C, 53.47; H, 3.79. Found: C, 53.43; H 3.88. Λ (THF, 24 °C): 0.18 S cm^2 mol^{-1}. IR (ν(CO), KBr): 2025, 1951, 1919, 1893, 1680 cm^{-1}. ^1H NMR (C_6D_6): δ 2.27 (s, 3H, $C(O)CH_3$), 1.6−1.9 (m, 4H, dppe CH_2), 7.0−7.6 (m, 20H, dppe C_6H_5). $^{31}P\{^1H\}$ NMR (C_6D_6): δ 24.1 (d, $^2J_{PP}$ = 45 Hz), 26.0 (d, $^2J_{PP}$ = 45 Hz). $^{13}C\{^1H\}$ NMR (C_6D_6): δ 25.4 (dd, J_{PC} = 23, 14 Hz, dppe CH_2), 27.3 (dd, J_{PC} = 27, 19

(19) (a) Komiya, S., Ed. *Synthesis of Organometallic Compounds: A Practical Guide*; Wiley: New York, 1997. (b) Shriver, D. F.; Drezdson, M. A. *The Manipulation of Air-Sensitive Compounds*, 2nd ed.; Wiley: New York, 1986.
(20) Kosolapoff, G. M.; Maier, L. *Organic Phosphorus Compounds*; Wiley: New York, 1972.
(21) Lapido, F. T.; Anderson, G. K. *Organometallics* **1994**, *13*, 303−306.
(22) Appleton, T. G.; Bennett, M. A.; Tomkins, I. B. *J. Chem. Soc., Dalton Trans.* **1976**, 439−446.
(23) Clark, H. C.; Manzer, L. E. *J. Organomet. Chem.* **1973**, *59*, 411−423.
(24) Piper, T. S.; Wilkinson, G. *J. Inorg. Nucl. Chem.* **1956**, *3*, 104−124.
(25) Edgell, W. F.; Lyford, J. *Inorg. Chem.* **1970**, *9*, 1932−1933.
(26) Ruff, J. K.; Schlientz, W. J. *Inorg. Synth.* **1974**, *15*, 84−90.

Hz, dppe CH_2), 39.1 (dd, J_{PC} = 42, 21 Hz, CH_3), 129−134 (m, dppe C_6H_5), 209−212 (m, CO), 235.0 (dd, J_{PC} = 115, 12 Hz, $C(O)CH_3$).

NMR Tube Reactions for CO Insertion. A typical procedure for **4** is given. CD_2Cl_2 (600 μL) was vacuum-transferred into an NMR sample tube (5 mmf × 180 mm) containing **4** (9.8 mg, 0.014 mmol), and 1,4-dioxane (0.5 μL) was added as an internal standard to the solution ([**4**] = 0.023 M). The solution was freeze−pump−thaw degassed, and CO (1 atm, ca. 9-fold excess of **4**) was introduced. The sample tube was placed in a thermostat at 24 ± 1 °C, and ^{1}H NMR spectra were periodically measured to follow the CO insertion reaction.

Reaction of 4 with dppe or PMe_3. A typical procedure for PMe_3 is shown. To a benzene solution of **4** (99.7 mg, 0.144 mmol) was added $P(CH_3)_3$ (0.145 mmol). Stirring at room temperature immediately gave a red oil and a yellow supernatant solution, and further stirring for 30 min yielded a red solution. The solution was evaporated to dryness, and the resulting solid was extracted with THF. After the filtered solution was again evaporated to dryness, the brown solids were washed with diethyl ether to give a white solid. The solid was recrystallized from a mixture of CH_2Cl_2 and Et_2O to give white crystals (57.7 mg, 0.0752 mmol). Yield: 52%. Anal. Calcd for $C_{34}H_{36}O_4P_3CoPd$: C, 53.25; H, 4.73. Found: C, 53.19; H, 4.23. IR (ν_{CO}, KBr): 1885, 1865 cm^{-1}. ^{1}H NMR (CD_2Cl_2): δ 0.48 (q, $^3J_{PH}$ = 6.4 Hz, 3H, CH_3), 1.21 (dd, J_{PH} = 9.5, 2.3 Hz, 9H, $P(CH_3)_3$), 2.41 (m, 4H, dppe CH_2), 7.0−7.6 (m, 20H, dppe C_6H_5). ^{31}P{^{1}H} NMR (C_6D_6): δ 12.0 (dd, $^2J_{PP}$ = 387, 34 Hz, $P(CH_3)_3$), 71.6 (dd, $^2J_{PP}$ = 34, 27 Hz, dppe P cis to $P(CH_3)_3$), 83.6 (dd, $^2J_{PP}$ = 387, 27 Hz, dppe P trans to $P(CH_3)_3$).

$[Pd_2(CH_3)_2(\mu\text{-dppe})(dppe)_2][Co(CO)_4]_2$ was obtained as pale yellow crystals from a mixture of CH_2Cl_2 and Et_2O. Yield: 82%. This complex was identified by spectroscopic methods. IR (ν(CO), KBr): 1878 cm^{-1}. ^{1}H NMR (CD_2Cl_2): δ 0.22 (br s, 6H, CH_3), 2.1−2.3 (m, 12H, dppe CH_2), 6.8−7.5 (m, 60H, dppe C_6H_5). ^{31}P{^{1}H} NMR (CD_2Cl_2): δ 22.4 (dm, $^2J_{PP}$ = 370 Hz, μ_2-dppe), 42.9 (dd, $^2J_{PP}$ = 32, 27 Hz, μ_1-dppe P trans to CH_3), 59.6 (dd, $^2J_{PP}$ = 370, 27 Hz, μ_1-dppe P cis to CH_3).

CO Insertion using ^{13}CO. 4 (56.0 mg, 0.0811 mmol) was dissolved in benzene in a Schlenk tube under N_2, and the solution was degassed. A known amount of ^{13}CO (2.22 mmol) was measured and adsorbed on dry silica gel at −196 °C using a manometer with a vacuum line. The ^{13}CO gas was introduced into the Schlenk tube, where the CO partial pressure was roughly 1 atm. The mixture was stirred at room temperature for 6 h, and the orange solution turned to red. The mixture was evaporated to dryness, and the resulting solid (**6***) was characterized by IR and NMR. Selected spectroscopic data for **6*** are as follows. IR (ν(CO), KBr): 2002, 1976, 1901, 1875, 1855, 1818, 1674, 1639 cm^{-1}. ^{31}P{^{1}H} NMR (C_6D_6): δ 24.2 (dd, $^2J_{PP}$ = 44, $^2J_{CP}$ = 115 Hz, P trans to $CH_3{}^{13}C(O)$, d, $^2J_{PP}$ = 44 Hz, P trans to $CH_3{}^{12}C(O)$), 25.9 (br d, $^2J_{PP}$ = 44 Hz, P trans to Co). ^{13}C{^{1}H} NMR (C_6D_6): δ 209−212 (m, CO), 235.0 (dd, $^2J_{PC}$ = 115, 12 Hz, $CH_3C(O)$).

Methods of Calculations. The B3LYP density functional theory was adopted in all the calculations.[27] In determining the structures of stationary points we used the LANL2DZ basis set implemented in the Gaussian series of programs, which consists of Los Alamos effective core potentials[28] for the Pd, Co, and P atoms and D95 split valence basis functions[29] for the C, O, and H atoms. Polarization functions were added on the P atoms.[30] This set of basis functions is called the basis set I. Using the structures thus determined, energy calculations were also carried out using the larger basis set II with d polarization functions[30] on the C and O atoms and f polarization functions[31] on the Pd and Co atoms, to obtain more reliable energetics. The optimized geometries of transition states (TSs) as well as equilibrium structures were characterized by normal-coordinate analysis, and the intrinsic reaction coordinates were followed to identify the reactant and product for each TS. The unscaled vibrational frequencies at the B3LYP/I level were used in the calculations of enthalpy. All the calculations were performed using the Gaussian 98 program.[32]

Acknowledgment. Part of the calculations were carried out at the Computer Center of the Institute for Molecular Science. This work was supported by a Grant-in-Aid for Scientific Research from the Ministry of Education, Science, Sports and Culture of Japan.

Supporting Information Available: Tables of crystal data and structure solution and refinement details, atomic coordinates, bond lengths and angles, and anisotropic thermal parameters for **4** and **5**. This material is available free of charge via the Internet at http://pubs.acs.org.

OM001037V

(27) (a) Becke, A. D. *Phys. Rev. A* **1988**, *38*, 3098−3100. (b) Lee, C.; Yang, W.; Parr, R. G. *Phys. Rev. B* **1988**, *37*, 785−789. (c) Becke, A. D. *J. Chem. Phys.* **1993**, *98*, 5648−5652.

(28) (a) Wadt, W. R.; Hay, P. J. *J. Chem. Phys.* **1985**, *82*, 284−298. (b) Hay, P. J.; Wadt, W. R. *J. Chem. Phys.* **1985**, *82*, 270, 299−310.

(29) Dunning, T. H., Jr.; Hay, P. J. In *Modern Theoretical Chemistry*; Schaefer, H. F., III, Ed.; Plenum: New York, 1976; Vol. 3, pp 1−29.

(30) Huzinaga, S.; Andzelm, J.; Klobukokowski, M.; Radzio-Andzelm, E.; Sakai, Y.; Tatewaki, H *Gaussian Basis Sets for Molecular Calculations*; Elsevier: Amsterdam, 1984.

(31) Ehlers, A. W.; Böhme, M.; Dapprich, S.; Gobbi, A.; Höllwarth, A.; Jonas, V.; Köhler, K. F.; Stegmann, R.; Veldkamp, A.; Frenking, G. *Chem. Phys. Lett.* **1993**, *208*, 111−114.

(32) Frisch, M. J.; Trucks, G. W.; Schlegel, H. B.; Scuseria, G. E.; Robb, M. A.; Cheeseman, J. R.; Zakrzewski, V. G.; Montgomery, J. A., Jr.; Stratmann, R. E.; Burant, J. C.; Dapprich, S.; Millam, J. M.; Daniels, A. D.; Kudin, K. N.; Strain, M. C.; Farkas, O.; Tomasi, J.; Barone, V.; Cossi, M.; Cammi, R.; Mennucci, B.; Pomelli, C.; Adamo, C.; Clifford, S.; Ochterski, J.; Petersson, G. A.; Ayala, P. Y.; Cui, Q.; Morokuma, K.; Malick, D. K.; Rabuck, A. D.; Raghavachari, K.; Foresman, J. B.; Cioslowski, J.; Ortiz, J. V.; Stefanov, B. B.; Liu, G.; Liashenko, A.; Piskorz, P.; Komaromi, I.; Gomperts, R.; Martin, R. L.; Fox, D. J.; Keith, T.; Al-Laham, M. A.; Peng, C. Y.; Nanayakkara, A.; Gonzalez, C.; Challacombe, M.; Gill, P. M. W.; Johnson, B. G.; Chen, W.; Wong, M. W.; Andres, J. L.; Head-Gordon, M.; Replogle, E. S.; Pople, J. A. *Gaussian 98*; Gaussian, Inc.: Pittsburgh, PA, 1998.